

An experimental method for quantifying tool–part shear interaction during composites processing

Graham Twigg, Anoush Poursartip*, Göran Fernlund

Department of Metals and Materials Engineering, The University of British Columbia, Vancouver, BC, Canada V6T 1Z4

Received 10 May 2002; received in revised form 27 March 2003; accepted 27 March 2003

Abstract

The success with which dimensional control during processing of composite structures can be modelled depends on the level of understanding of the underlying mechanisms that drive the accumulation of residual stresses in the part. Tool–part shear interaction during processing can cause substantial warpage in initially flat laminates, yet this phenomenon remains poorly understood. This paper presents an experimental technique in which a thin tool, instrumented with strain gauges, is used for characterizing the interfacial shear stresses that arise between the tool and part during processing. The results show that a sliding interface condition occurs during the majority of the cure cycle, although, at times the tool and part adhere together resulting in high interfacial shear stresses. This tool–part interaction occurs despite the use of a release agent, though the use of a fluoroethylenepropylene (FEP) release film at the tool–part interface reduces the effect.

© 2003 Elsevier Ltd. All rights reserved.

Keywords: Tool–part interaction; A. Polymer-matrix composites; C. Residual stress; C. Stress transfer

1. Introduction

For the affordable structures demanded in modern commercial applications, the high initial cost of composite materials must be offset by savings in other steps of the manufacturing process. A key aspect to this cost-effective manufacturing approach is the ability to fabricate composite components with accurate dimensions. Residual stresses and the dimensional inaccuracies they cause are to a certain extent an unavoidable consequence of the autoclave process. However, through the use of process models the tool designer can potentially account for these deformations, eliminating the need for tool revisions or assembly shims. The success of these process models is highly dependent on having a good understanding of the mechanisms by which the residual stresses accumulate during processing and, in turn, accurately representing these mechanisms in the models.

The problem of residual stress and associated shape change is complex because of the large number of sources

of residual stress and the potential for interaction between them. Of the sources commonly identified, those involving laminate anisotropy have been studied most thoroughly. However, there commonly exists a component of shape change that is not attributable to laminate anisotropy. In particular, thin, balanced laminates fabricated on flat tooling are often seen to exhibit a concave down warpage after processing. This is often attributed to a mismatch between tool and part coefficient of thermal expansion (CTE) and associated tool–part interaction [1–3].

The mechanism put forth considers a low CTE laminate against a tool with a considerably higher CTE. When the tool and part are forced together due to autoclave pressure and subjected to a temperature ramp, a shear interaction between the tooling and the curing part arises which places the laminate in tension. As this occurs prior to any significant degree of resin modulus development, the laminate shear modulus is very low and plies that are distant from the tooling are not loaded to the same extent as those close to the interface. This non-uniform stress distribution is locked in as the resin cures, and upon removal from the tooling, the resultant bending moment warps the part away from the tooling.

* Corresponding author. Tel.: +1-604-822-3665; fax: +1-604-822-3619.

E-mail address: anoush@composites.ubc.ca (A. Poursartip).

Efforts to incorporate tool–part interaction behaviour into process models have shown that it can have a tremendous influence on the magnitude of predicted deformations [4]. At the present time though, there is a lack of experimental basis for the selection of input parameters for these models [5]. The typical approach to model tool–part interaction involves calibration by matching the model predictions to an actual deformed part shape. To date only a few studies have attempted to experimentally characterize the nature of the shear interaction between the tool and part.

In a study of the compaction and flow of composite laminates, an environmental scanning electron microscope was used to observe the tool–part interfacial region of a laminate during processing [6]. The procedure involved compacting a laminate between two plates, thereby forcing the material to flow perpendicular to the applied load. By monitoring the migration of tungsten markers placed at locations throughout the laminate, the change in displacement profile with respect to time was determined. This displacement profile in turn could be related to the interfacial conditions. The experiments were performed at a temperature of approximately 50 °C so the conditions were only representative of the very early portion of the cure cycle. However, this technique yielded the interesting result that both sliding and sticking conditions can occur at the tool–part interface.

As part of a comprehensive effort to model process induced deformations, friction coefficients for a carbon/epoxy pre-preg material have been characterized at a variety of temperatures and pressures [7]. The critical interfacial shear stress at which sliding occurred was assumed to follow the classical friction relation:

$$\tau_{Cr} = \mu \cdot P \quad (1)$$

where τ_{Cr} is the critical interfacial shear stress, μ is the coefficient of friction and P is the pressure acting normal to the interface. A test apparatus was developed which simulated the effect of autoclave pressure and vacuum bagging by applying dead weight loading to a laminate stack up to an equivalent pressure of 240 kPa (35 psi). The force required to pull a ply from the laminate stack was measured, from which friction coefficients were determined for the cases of a tool coated with release agent (FreeKote), a tool covered with a fluoroethylenepropylene (FEP) release ply and for the interface between two plies. The friction coefficients (μ) were found to be insensitive to pressure but they increased significantly with temperature. The release agent tool–part interface had higher associated μ values than the FEP interface, ranging from 0.18–0.32 and 0.07–0.21 respectively.

Researchers in our laboratory have developed a qualitative means of examining the interactions between tool and part during processing by mounting a strain

gauge rosette on a thin aluminium tool [8]. A stack of pre-preg was placed on the opposite side of the tool plate and the tool and part were enveloped in a vacuum bag and subjected to a cure cycle during which time the strain in the tool was measured. No external autoclave pressure was applied to the curing assembly. In one case, the experiment was performed with a roughened tool surface and no release agent at the interface, while in the other case two sheets of Mylar release film were placed at the tool–part interface.

The conclusion of the experiment was that prior to gelation, there was no appreciable mechanical interaction between tool and part, regardless of tool surface condition. This was indicated by the fact that the strain measured in the tool–plate was approximately the same as that due to the free thermal expansion of the aluminium tool. After part gelation, for the untreated interface, changes in strain as a function of temperature were more representative of longitudinal and transverse CTEs of the CFRP part rather than the CTE of the aluminium plate indicating a high degree of stress transfer between the tool and part. The use of the Mylar film at the interface prevented any significant interaction regardless of degree of cure.

Tool–part interaction is clearly dependent on several process parameters and is difficult to measure directly. This paper presents a method for experimentally measuring both the distribution and magnitude of tool–part interfacial shear stress during autoclave processing. The nature and the build-up of interfacial shear stresses is presented for different process conditions.

2. Instrumented tool approach

Stress cannot be measured directly, but the interfacial shear stress acting on a body may be inferred from the normal strains exhibited by material close to the interface. Strain gauges are sufficiently robust to survive an autoclave cycle, hence they are well suited for this type of measurement. When examining this interfacial phenomena one has the option of examining strains from the tool side or from the part side. Strain gauge placement in the part itself has been utilized successfully for the examination of residual stresses that arise after part gelation but there are inherent difficulties in this technique [9]. For this reason, it was decided to place strain gauges on the tool itself.

To ensure that the magnitudes of the strain induced in the tool were sufficiently large to be measurable, a thin, compliant tool was used. Several gauges were placed along the length of the tool and the constraint or stretching to which the tool was subjected during the entire process cycle was monitored. From this measurement it is possible to estimate the magnitude and distribution of shear stresses at the tool–part interface.

3. Experimental

The instrumented tool was a 6061-T6 aluminium plate with dimensions of 100 mm × 600 mm × 0.762 mm. Eight strain gauges were placed on the tool, six oriented longitudinally and two transversely, as shown in Fig. 1. The eight Micro Measurements EA-13-250BG-120-Option-LE gauges were adhesively bonded to the aluminium tool using Micro Measurements M-Bond 43B adhesive. The pre-attached leadwires were soldered to 26 AWG wires for connection to a data acquisition (DAQ) system.

A [0]₁₆ CFRP (T-800H/3900-2) part with the same length and width as the instrumented tool was placed on a 6.35 mm thick aluminium baseplate. Two sheets of FEP separated the part and the baseplate. The instrumented tool was then placed on top of the CFRP part. The assembly was vacuum bagged and subjected to a slightly modified version of a standard 180 °C (355 °F) cure cycle. The modifications to the cure cycle are discussed shortly. Two interface and two pressure conditions were examined:

1. Two plies of FEP, and Freekote release agent.
2. 103 and 586 kPa autoclave pressures.

As the cure cycle progressed, strains measured in the thin tool were recorded with the DAQ system. Compensation for the free thermal output of the strain gauges was performed subsequently using experimentally determined calibration constants. The long-term stability of the strain gauge calibration was confirmed by repeating the calibration at a later date. The product of this experimental technique is a history of the in-plane, mechanical strain in the thin tool throughout the cure cycle. The experimental error associated with this technique is estimated to be ±9µε.

Before presenting the results, a brief explanation of the temperature cycle used is warranted. The state of mechanical strain in the thin tool changes mainly when

the tool part assembly is subjected to a change in temperature. To provide greater insight into the progress of tool–part interaction during the isothermal portion of the cure cycle in particular, temperature modulations were programmed into the autoclave controller. These temperature dips were also used during the heat-up portion of the cure cycle. A typical thermal cycle used is shown in Fig. 2 along with the predicted part degree of cure and resin modulus. Predictions of part degree of cure and resin modulus were done using established cure kinetics and modulus development equations for the material (based on DSC and DMA measurements, respectively). The resin modulus is dependent on both the degree of cure and temperature as shown in Fig. 2. The model used for process simulations is presented in Ref. [10]. The autoclave pressure was held constant during cool-down of the part to promote tool–part interaction.

4. Instrumented tool theory

If there is a CTE mismatch between tool and part, there will be a driving force for shear stress development at the tool–part interface. This driving force can be represented by the mismatch strain, $\epsilon_{\text{Mismatch}}$, which is the difference between the unconstrained thermal expansion of the tool and part:

$$\epsilon_{\text{Mismatch}} = (\text{CTE}_{\text{Tool}} - \text{CTE}_{\text{Part}}) \cdot (\Delta T) \quad (2)$$

where CTE_{Tool} and CTE_{Part} are the respective thermal expansion coefficients and ΔT is the temperature change. The strain data generated from the instrumented experiments represents the in-plane, mechanical strain induced in the tool due to this shear interaction. The following section presents the theory by which the tool–part interface conditions can be related to the measured in-plane strains. For the scope of this study it is sufficient to consider two interface conditions: the sliding friction condition and the sticking interface condition.

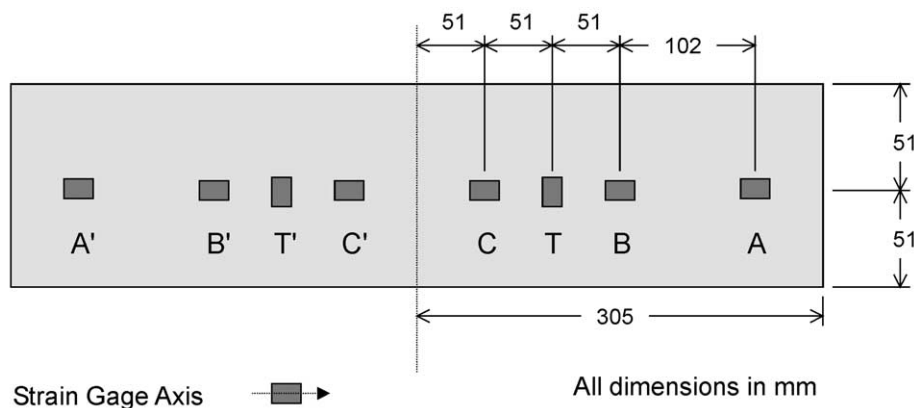


Fig. 1. Arrangement and designation of strain gauges on instrumented tool.

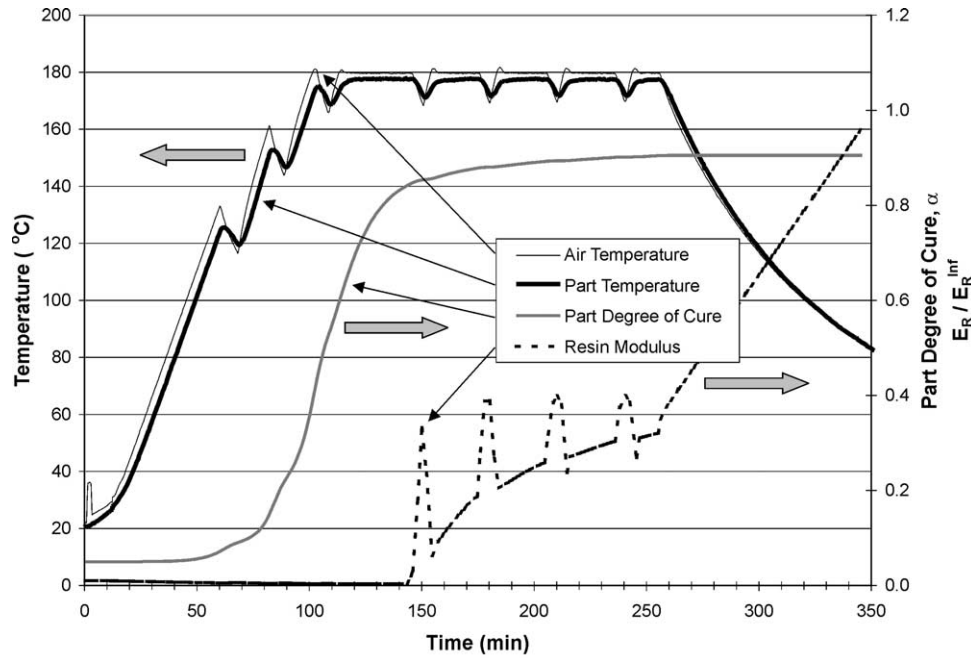


Fig. 2. Typical thermal cycle used for the instrumented tool experiments.

Regardless of the interface condition present, the following assumptions are implicit in the thin instrumented tool approach used here. Firstly, it is assumed that temperatures are constant along the part length. This assumption was confirmed by experiments, where it was shown that temperatures did not vary more than 1 °C over the entire part length. Secondly, it is assumed that through-thickness in-plane strain gradients in the thin tool are negligible, i.e. the strains induced at the tool part interface are equal in magnitude to the strains measured on the free surface of the tool. This assumption is based on the fact that the tool thickness is small, and the tool shear modulus is relatively high, so the decay of strain through the instrumented tool thickness is minimal. Finally, it is assumed that the instrumented tool is not subject to bending deformations which would cause erroneous strain readings. Bending deformations will occur in a bi-material strip subjected to a temperature change, if it is not constrained in the out-of-plane direction. However, as the instrumented tool–part assembly was forced against the baseplate by autoclave pressure, no out-of-plane bending deformations were possible.

4.1. Sliding friction condition

The first theoretical case for consideration is that of the sliding frictional interface. This condition implies that the shear stress along the entire tool–part interface is a constant value. The magnitude of the shear stress is often assumed to be proportional to the normal stress acting on the interface, as suggested by the Coulomb friction model:

$$\tau_{\text{Sliding}} = \mu \cdot P \quad (3)$$

where τ_{Sliding} is the interfacial shear stress, μ is the dimensionless friction coefficient and P is the autoclave pressure. It is important to note that under these conditions, the interfacial shear stress will be independent of $\varepsilon_{\text{Mismatch}}$, see Eq. (2).

A free-body diagram of half a thin tool of length $2L$ is shown in Fig. 3. Examining the force equilibrium on a tool element with dimensions t_{Tool} by dx by unit depth yields the following:

$$(\sigma_{xx} + d\sigma_{xx} - \sigma_{xx}) \cdot t_{\text{Tool}} + \tau_{xz} \cdot dx = 0 \quad (4)$$

In the remaining text, the subscripts for the stress terms will be omitted, hence σ_{xx} is referred to simply as σ and τ_{xz} as τ . Rearranging gives:

$$d\sigma = \frac{-\tau}{t_{\text{Tool}}} \cdot dx \quad (5)$$

$$\int_0^\sigma d\sigma = \int_L^x \frac{-\tau}{t_{\text{Tool}}} \cdot dx \quad (6)$$

In the case of sliding friction $\tau = \tau_{\text{Sliding}}$ along the entire interface, integration of Eq. (6) yields:

$$\sigma = \frac{\tau_{\text{Sliding}} \cdot (L - x)}{t_{\text{Tool}}} \quad (7)$$

The shear stress and in-plane stress distributions for this condition are shown schematically in Fig. 4. The mechanical strains as measured by the gauges are related to the in-plane stress by the Young's modulus, E_{Tool} , of the thin tool. The mechanical strain is the total strain minus the free thermal expansion.

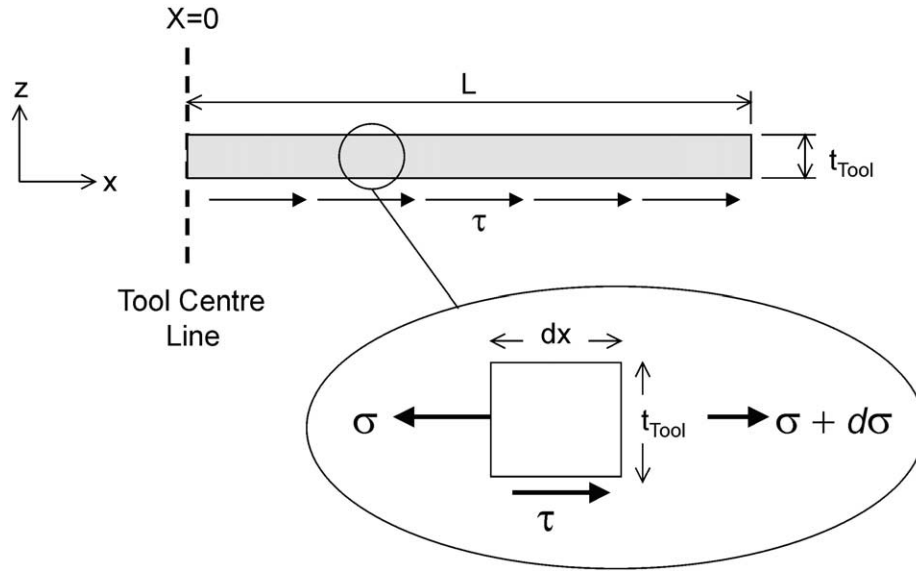


Fig. 3. Free-body diagram of half of a thin tool under sliding friction conditions.

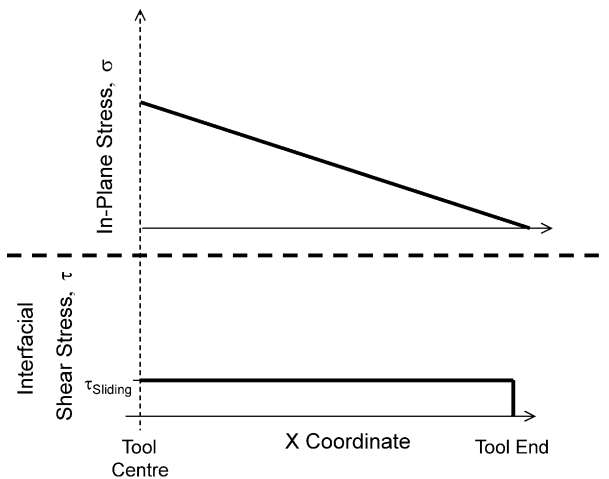


Fig. 4. Interfacial shear and in-plane stress distributions for the case of a sliding friction interface.

$$\varepsilon = \frac{\tau_{\text{Sliding}} \cdot (L - x)}{E_{\text{Tool}} \cdot t_{\text{Tool}}} \quad (8)$$

Considering Eq. (8) in the context of the instrumented tool experiment, in the case that sliding friction is prevalent at the interface and the tool–part combination is subjected to a temperature change, the following characteristic behaviour should be observed:

- Strain magnitudes as measured by the gauges should be directly proportional to their distance from the end of the tool.
- Strain magnitudes should be independent of $\varepsilon_{\text{Mismatch}}$, and hence independent of the temperature change to which the tool–part assembly is subjected. The exception to this would be the case in which τ_{Sliding} is increasing at the same

time the tool–part assembly is subjected to a temperature change.

4.2. Stick condition

The second interface condition to be considered is that representing sticking or adhesion between the tool and part. Solutions for similar problems in adhesive bonding research have been developed so these will serve as a basis for the development presented here, see Ref. [11]. This situation also has many similarities to the stress transfer that occurs between fibre and matrix in a composite material. This class of problem is often analysed using a shear lag approach. Consider the general case of two elastic adherends separated by an adhesive layer, with geometries as shown in Fig. 5. The adherends (tool and part) are assumed to undergo no shearing, while the adhesive is assumed to experience no extensional strains. Examining the force equilibrium on an element dx in length by unit depth gives (Fig. 5):

$$\tau = -\frac{d\sigma_1}{dx} \cdot h_1 = \frac{d\sigma_2}{dx} \cdot h_2 \quad (9)$$

Considering Hooke’s law and the strain–displacement relation, one can relate the stresses in the adherends to their displacements:

$$\frac{du_1}{dx} = \varepsilon_1 = \frac{\sigma_1}{E} + \text{CTE}_1 \cdot \Delta T \quad (10a)$$

$$\frac{du_2}{dx} = \varepsilon_2 = \frac{\sigma_2}{E} + \text{CTE}_2 \cdot \Delta T \quad (10b)$$

where u_1 and u_2 are the displacements of the bottom and top adherends, respectively, E is the modulus of the

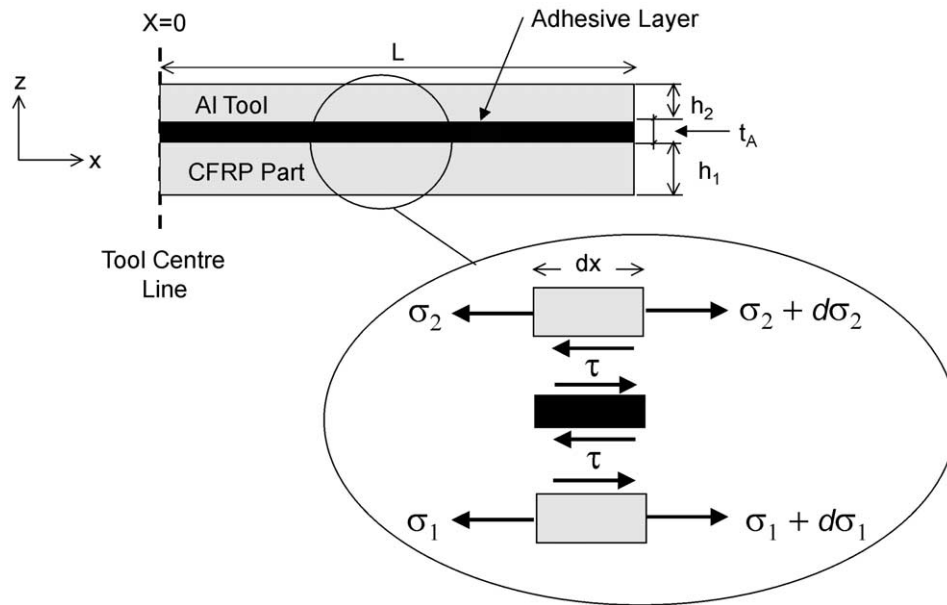


Fig. 5. Geometry of the thin tool loading under sticking interface conditions.

adherends and CTE_1 and CTE_2 are the respective coefficients of thermal expansion. Differentiating and incorporating Eq. (9) gives:

$$\frac{d^2 u_1}{dx^2} = \frac{d\sigma_1}{dx} \cdot \frac{1}{E} = -\frac{\tau}{E \cdot h_1} \tag{11a}$$

$$\frac{d^2 u_2}{dx^2} = \frac{d\sigma_2}{dx} \cdot \frac{1}{E} = \frac{\tau}{E \cdot h_2} \tag{11b}$$

Now considering the adhesive layer:

$$\tau = G \cdot \gamma = G \cdot \frac{u_2 - u_1}{t_A} \tag{12}$$

where G is the shear modulus of the adhesive layer. Differentiating Eq. (12) twice and incorporating Eqs. (11a) and (11b) gives a differential equation for τ :

$$\frac{d^2 \tau}{dx^2} = \tau \cdot \frac{G \cdot (h_1 + h_2)}{E \cdot t_A \cdot h_1 \cdot h_2} \tag{13}$$

With the boundary conditions $\tau(0)=0$, and $\sigma_1(L)=\sigma_2(L)=0$, the solution of this equation is:

$$\tau = (e^{\lambda x} - e^{-\lambda x}) \cdot \frac{G \cdot (CTE_2 - CTE_1) \cdot \Delta T}{t_A \cdot \lambda \cdot (e^{\lambda L} + e^{-\lambda L})} \tag{14}$$

where:

$$\lambda = \sqrt{\frac{G \cdot (h_1 + h_2)}{E \cdot t_A \cdot h_1 \cdot h_2}} \tag{15}$$

Putting representative values into Eq. (14) yields an interfacial shear stress distribution as shown in Fig. 6. This is characterized by a very low shear stress over much of the interface length, with the shear stress increasing exponentially over a short region near the

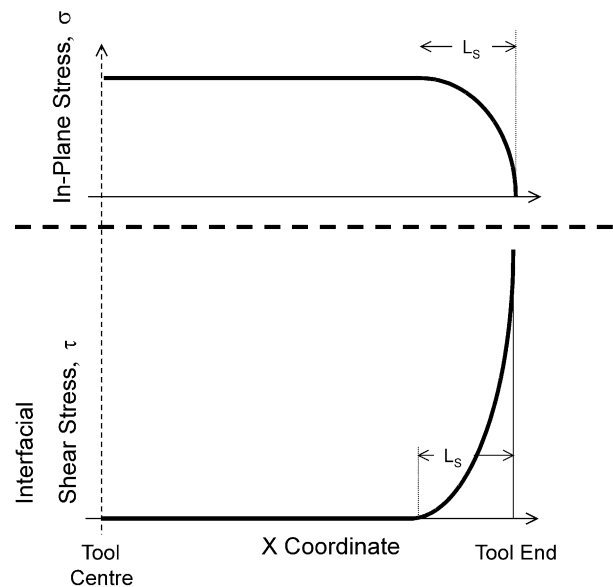


Fig. 6. Schematic of the interfacial shear and in-plane stress distributions for the case of a perfectly bonded tool-part interface.

end of the interface. This region is referred to as the stress transfer length, L_s . Given Eq. (14) it is apparent that the magnitude of the shear stress is proportional to the $\epsilon_{Mismatch}$ term from Eq. (2).

Recalling Eq. (6), and incorporating Hooke's law gives:

$$\epsilon \cdot E = \sigma = \frac{1}{t_{Tool}} \int_L^x -\tau \cdot dx \tag{16}$$

where ϵ is the mechanical strain, which is the total strain minus the free thermal expansion. Eq. (16) states that the in-plane stress and strain at a given point will be

proportional to the integral of the shear stress from the interface end to that point. The in-plane stress distribution corresponding to the perfect bonding condition is also shown schematically in Fig. 6. Based on this distribution, for the sticking interface condition one can expect strain in the tool to develop as follows:

- Strains in the thin tool will be constant along the length, unless the gauges are located close enough to the tool end to be within the zone over which the shear stress is building (the stress transfer length L_s).
- The magnitude of the interfacial shear stress and hence the in-plane strain, will increase as the $\varepsilon_{\text{Mismatch}}$ term increases. A temperature change will thus cause tool strains to increase.
- The interfacial shear stress will be a maximum at the tool end.

The sliding friction and sticking interface conditions are analogous to plastic and elastic material deformations, respectively. In most processes, the interface condition is likely a combination of stick and slip, as will be demonstrated in this paper. A schematic illustration of interfacial shear stress versus interface displacement, $\delta_{\text{Interface}}$, for an arbitrary point along the tool–part length is shown in Fig. 7. At low values of $\delta_{\text{Interface}}$, the elastic condition governs, with τ being proportional to $\delta_{\text{Interface}}$. As $\delta_{\text{Interface}}$ increases so does τ , until it reaches the critical shear stress for debonding, τ_{Debond} . After debonding, the sliding condition is in effect, thus as $\delta_{\text{Interface}}$ is increased further, the interfacial shear stress remains constant at τ_{Sliding} .

5. Instrumented tool results

The results from the 586 kPa autoclave pressure/Release Agent interface condition experiments will be presented in detail after which the results from other

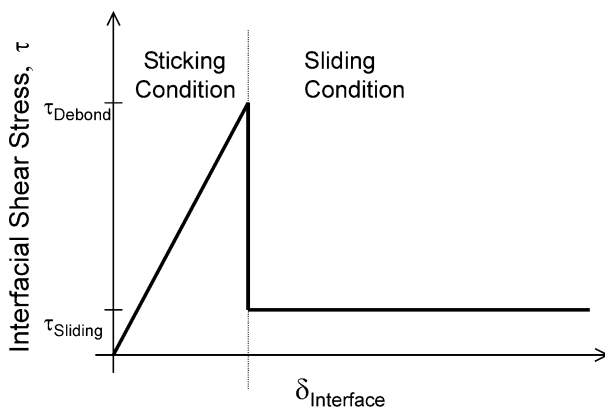


Fig. 7. Theoretical interfacial shear stress development as a function of interface displacement.

conditions can be compared. Fig. 8 shows the measured evolution of mechanical strain in the thin tool throughout the cure cycle. Only gauges from one side of the tool symmetry line are shown for the sake of clarity. Again it should be emphasized that the strains shown in all plots have their free thermal output removed, meaning that the strains depicted are those corresponding directly to stresses in the thin tool.

5.1. Strain development—cool-down

While the end of the cure cycle is not expected to be significant in terms of developing residual stresses in the part, it is instructive to examine the experimental results starting with the cool-down portion of the cure cycle because the strain magnitudes are very large making trends easier to identify. Furthermore, at this time the part degree of cure is unchanging and part properties can be reasonably assumed to be fully elastic.

An expanded view of the cool-down portion of the cycle is shown in Fig. 9. The CTE of the aluminium tool is approximately $24 \mu\text{E}/^\circ\text{C}$ compared with 0 and $44 \mu\text{E}/^\circ\text{C}$ for the CFRP in the longitudinal and transverse directions, respectively. The thermo-elastic properties of the CFRP laminate and aluminium tool used for calculation purposes are shown in Table 1. Despite the use of a release agent, as the tool and part cool, the two are perfectly bonded. In the longitudinal direction the aluminium tool is prevented from freely thermally contracting, resulting in a tensile stress which increases as the temperature drops further from the cure temperature. In the transverse direction the opposite trend is seen owing to the greater CTE of the part than the tool in that direction. The strain in the toolplate continues to increase until a sharp discontinuity occurs. The discontinuity is associated with debonding of the tool and part.

Debonding occurs in a manner consistent with theory for a perfectly bonded bi-material strip. Recall from Section 4.2 that for the elastic distribution, the interfacial shear stress is expected to be zero over most of the part length but increases to a maximum over a short region near the tool end, while the resulting in-plane strain should be constant over most of the tool length. Experimentally, it is observed that as the cooling progresses, in-plane strains build at the same rate for each gauge location. Debonding occurs first at the part end, where interfacial shear stress is a maximum. The debond front then progresses towards the part centre, reflected by the order in which the gauges debond. After debonding, the in-plane strain drops considerably and then remains constant as the temperature drops further. The gauges show a strain level proportional to their distance from the tool end suggesting that after debonding, a sliding friction interface condition is operative for the rest of the cool-down (note that the autoclave pressure remains applied for the entire duration of the cool-down). This results in

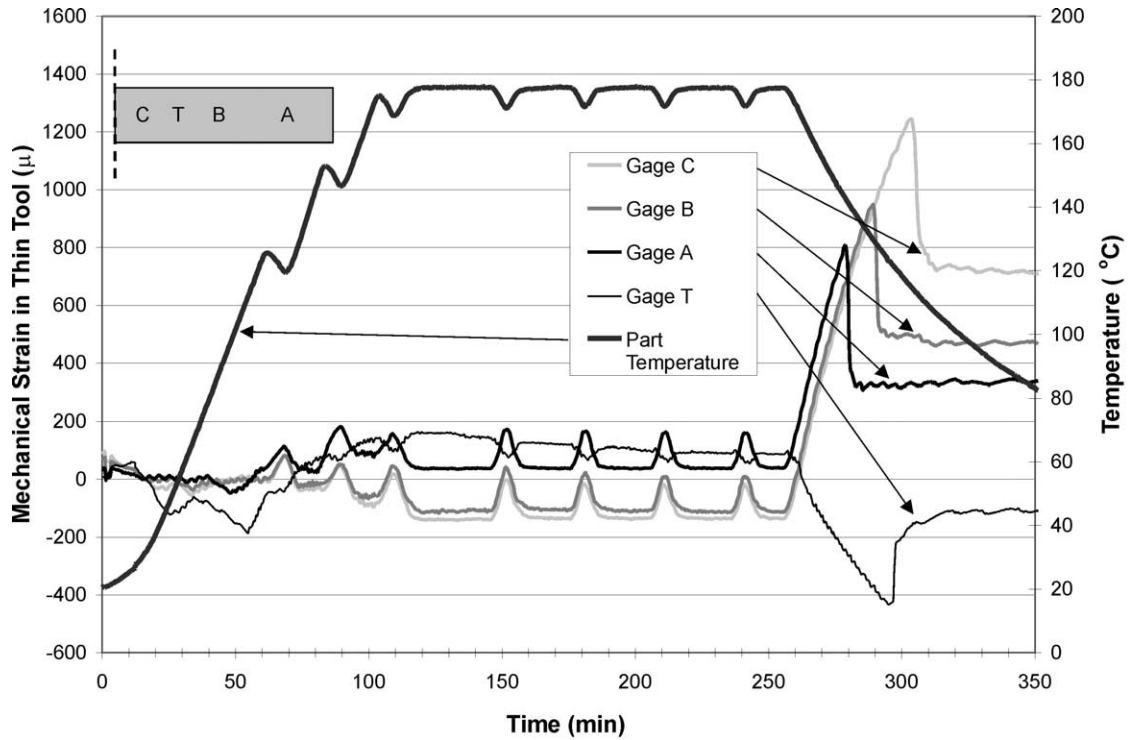


Fig. 8. Mechanical strain evolution in the instrumented tool for the entire process cycle. 586 kPa autoclave pressure/release agent interface.

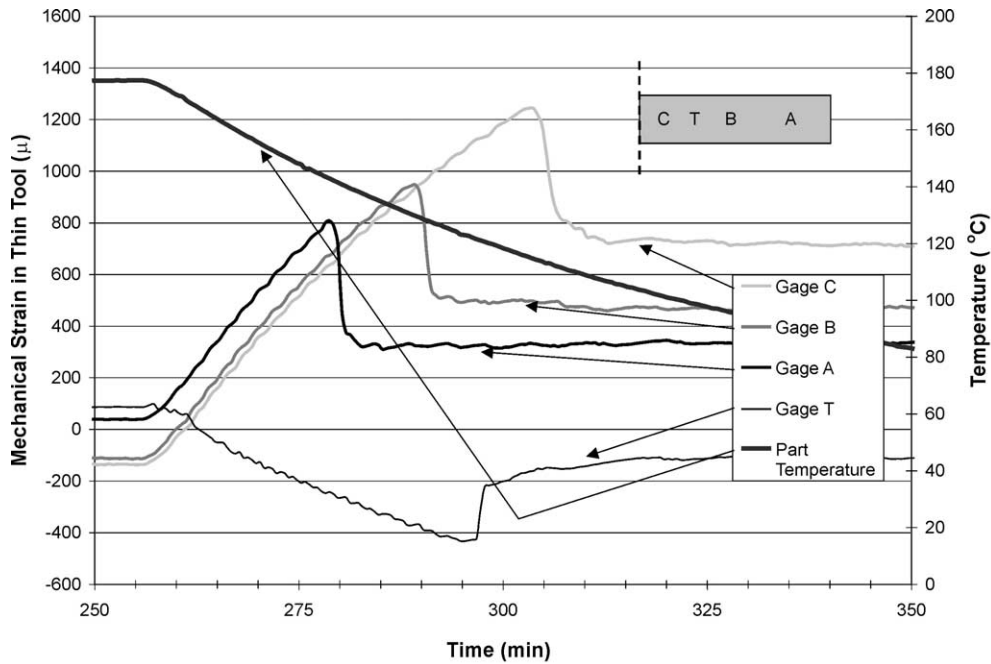


Fig. 9. Mechanical strain evolution during the cool-down portion of the cure cycle. 586 kPa autoclave pressure/release agent interface.

Table 1
Material properties used for calculation purposes expressed as a function of temperature

Material	T-800/3900-2 Longitudinal	T800/3900-2 Transverse	Aluminium 6061-T6
Young's Modulus E (GPa)	126–0.0154 (T-20)	9.7–0.0369 (T-20)	69
CTE (m/°C)	0.0374–0.000786 (T-20)	33.3 + 0.0894 (T-20)	22.3 + 0.0204 (T-20)

Note that *T* refers to the temperature in °C.

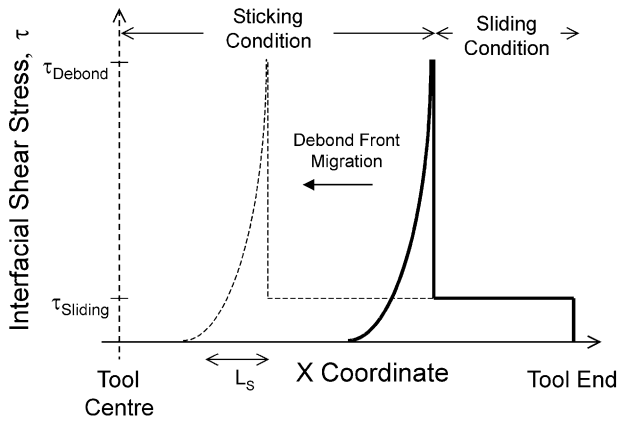


Fig. 10. Illustration of interfacial shear stress distribution as the debond front travels from the tool end towards the centre.

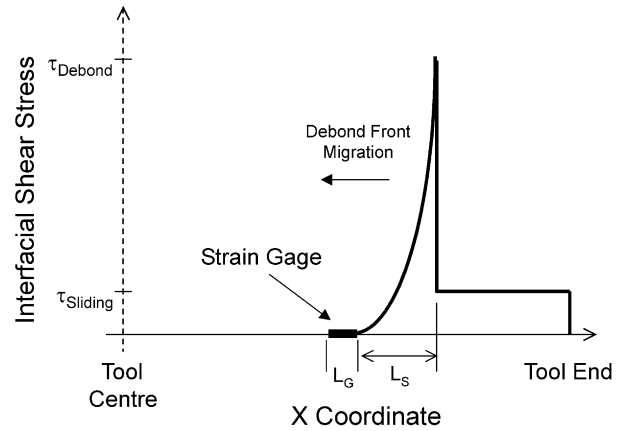


Fig. 11. Interfacial shear stress distribution corresponding to the peak strain gauge reading prior to debonding.

part of the interface being subjected to the sliding friction condition while the rest remains adhesively bonded as illustrated in Fig. 10.

5.1.1. Estimate of L_S

Having first developed a qualitative understanding of the distribution of interfacial shear stress, it is possible to determine the magnitudes of τ_{Debond} , L_S and τ_{Sliding} . The peak strain that a given gauge reads immediately prior to debonding, ϵ^i , occurs the instant prior to the stress transfer length, L_S , reaching that gauge. The interfacial shear stress distribution corresponding to this situation is shown in Fig. 11. The plateau strain value after debonding, ϵ^f , is reached at the moment when L_S has travelled past the gauge, corresponding to Fig. 12. It is important to note that the finite dimensions of the strain gauge are significant in the following arguments. In the period over which the strain is dropping from ϵ^i to ϵ^f , the debond front travels a total distance of Δx :

$$\Delta x = L_S + L_G \tag{17}$$

where L_G is the active gauge length¹ of the strain gauge. For the gauges considered in the present work, the active gauge length was 6.4 mm.

The distance Δx , and hence the stress transfer length, L_0 , can be calculated based on two related quantities: the temperature span of the debond event, ΔT , and the rate of debond migration with respect to temperature, $\frac{\Delta x}{\Delta T}$. Both these quantities are readily identified from the experimental output, enabling a calculation of L_S as follows:

$$L_S + L_G = \Delta x = \frac{\Delta x}{\Delta T} \cdot \Delta T \tag{18}$$

$$L_S = \frac{\Delta x}{\Delta T} \cdot \Delta T - L_G \tag{19}$$

¹ The active gauge length is considered as opposed to the overall length of the gauge including the backing.

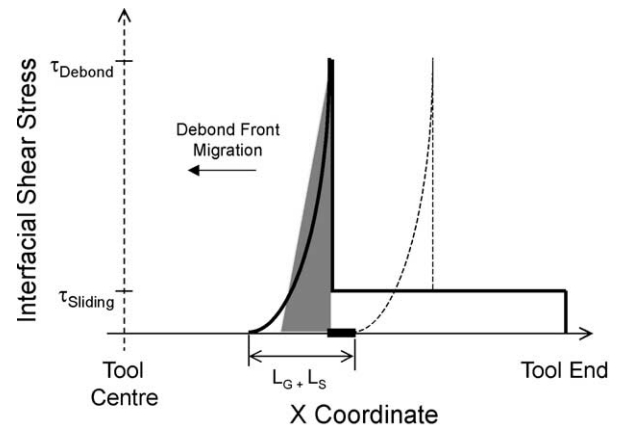


Fig. 12. Interfacial shear stress distribution corresponding to the post-debond plateau strain gauge reading.

This calculation is performed with respect to *temperature* rather than *time* because as will be seen, the debond migration rate is constant with respect to temperature whereas it varies with respect to time.

Fig. 13 examines the strain evolution at a single gauge during debonding, illustrating that this event actually occurs over a period of approximately 2 min. Alternatively one can express the duration of this event in terms of the temperature span, ΔT , over which it occurs. The average temperature span for L_S to pass a given gauge was 2.8 °C.

Recall that the peak strain which a gauge reads occurs the instant prior to L_S reaching that gauge. This enables one to identify the exact location of the debond front at four separate moments during the cool-down. Fig. 14 shows a plot of debond front location versus tool temperature. The slope of this line, $\frac{\Delta x}{\Delta T}$, represents the debond front migration rate. From this plot it is apparent that the debond migration rate of 7.1 mm/°C is constant with respect to temperature. Incorporating these values into Eq. (19) gives:

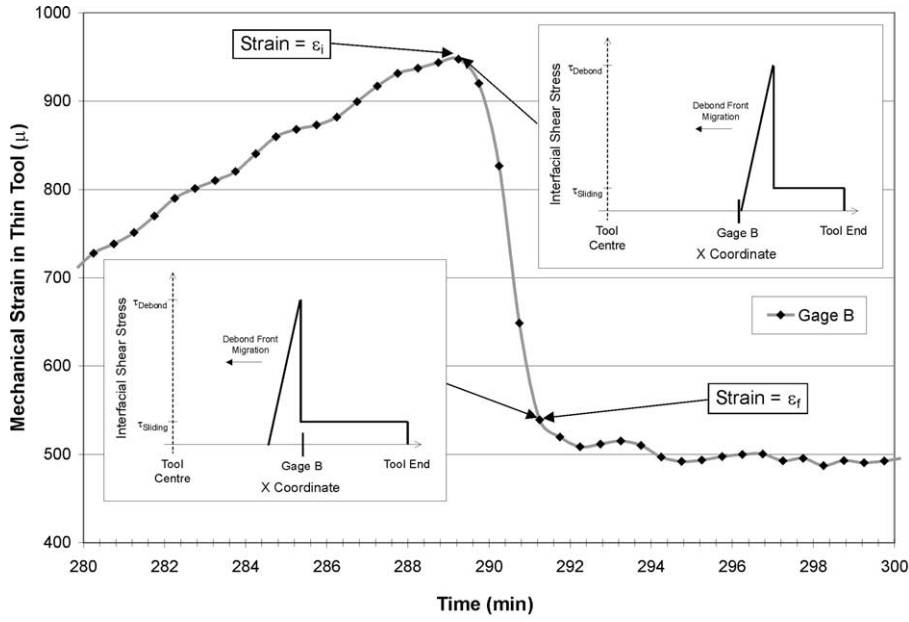


Fig. 13. Strain evolution at a single gauge during the debond event.

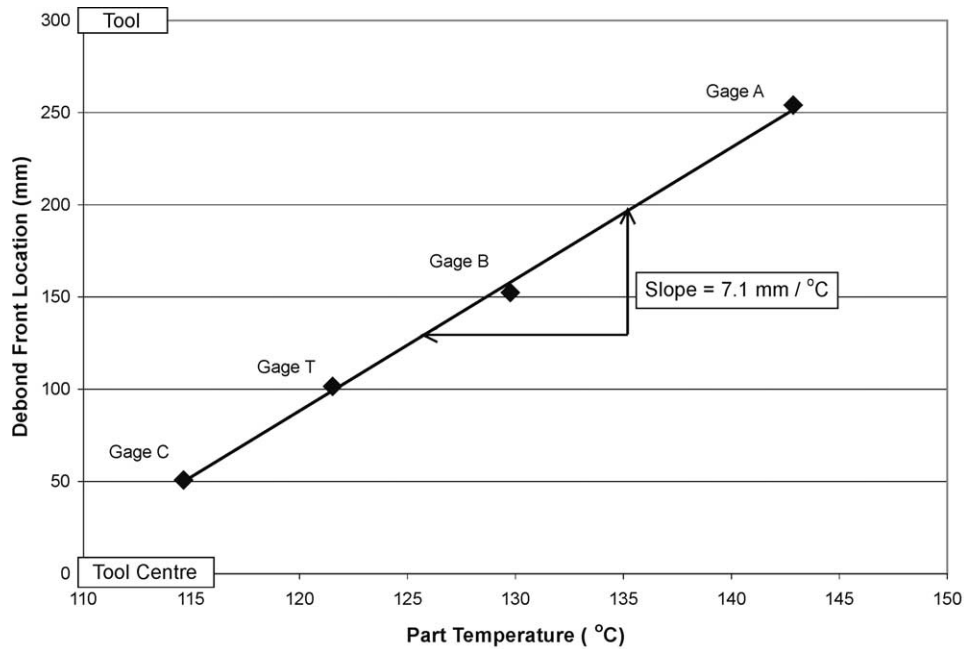


Fig. 14. Debond front migration with respect to part temperature.

$$L_S = 7.1 \frac{\text{mm}}{^\circ\text{C}} \cdot 2.8^\circ\text{C} - 6.35 \text{ mm} = 14 \text{ mm} \quad (20)$$

5.1.2. Estimate of τ_{Debond}

Now that an estimate of the stress transfer length L_S is available, one can also calculate τ_{Debond} . Recalling Eq. (6), one can relate the strain measured by a gauge to the integral of the shear stress between the interface end and the gauge location, x :

$$\varepsilon = \frac{1}{t_{\text{Tool}} \cdot E_{\text{Tool}}} \int_L^x -\tau \cdot dx \quad (21)$$

The change in strain measured by the gauge during the debond event can thus be related to the change in the integral of the shear stress.

$$\begin{aligned} \Delta\varepsilon &= \varepsilon^f - \varepsilon^i \\ &= \frac{1}{t_{\text{Tool}} \cdot E_{\text{Tool}}} \cdot \left[\left\{ \int_L^x -\tau \cdot dx \right\}^f - \left\{ \int_L^x -\tau \cdot dx \right\}^i \right] \quad (22) \end{aligned}$$

During the cool-down, the shear stress distribution cannot be described by a single integrable function, but a reasonable approximation of the required quantities can be determined by estimating areas from schematic τ versus x coordinate curves. Recall that Fig. 11 shows the shear stress distribution corresponding to the time at which the peak strain, ε^i , is recorded at a given gauge, while Fig. 12 corresponds to the post debond value, ε^f . As L_S passes a given gauge, the area under the curve between the interface end and the gauge changes by an amount approximately equal to the area of the shaded triangle in Fig. 12. Moreover, in the event that $\tau_{\text{Debond}} > \tau_{\text{Sliding}}$, this area can be approximated as follows:

$$\left\{ \int_L^x -\tau \cdot dx \right\}^f - \left\{ \int_L^x -\tau \cdot dx \right\}^i \approx \frac{1}{2} \cdot \tau_{\text{Debond}} \cdot L_S \quad (23)$$

Combining Eqs. (22) and (23) and solving for τ_{Debond} gives:

$$\tau_{\text{Debond}} = \frac{2 \cdot (\varepsilon_f - \varepsilon_i) \cdot t \cdot E}{L_S} \quad (24)$$

Using an average value for $(\varepsilon_f - \varepsilon_i)$ and the value for L_S as calculated earlier yields an estimate of τ_{Debond} of 3.8 MPa. For comparison, the bond strength for metal adherends with a typical structural epoxy adhesive can be expected to be of the order of 22–40 MPa.

5.1.3. Estimate of τ_{Sliding}

Finally, the magnitude of τ_{Sliding} can be estimated from the strain measurements during the post debond period. Differentiating Eq. (8) and rearranging gives:

$$\tau_{\text{Sliding}} = \frac{-d\varepsilon}{dx} \cdot E \cdot t \quad (25)$$

A plot of post debond strain versus gauge location is shown in Fig. 15 (note that results are also shown for other periods during the cure cycle, during which a sliding interface condition is occurring). The strain value reported for a given location is the average of appropriate gauges on both sides of the part symmetry line. A straight line was fitted to the data, and forced to go through zero strain at the tool end (to reflect the fact that the tool is stress free at the end). The slope of the line in Fig. 15 represents $\frac{d\varepsilon}{dx}$, and applying values of 70 GPa and 0.762 mm for the tool modulus and thickness respectively yields a value for τ_{Sliding} of 167 kPa. The error associated with this technique was determined from the effect which the strain measurement error had on the slope estimate. The strain measurement error of $\pm 10 \mu\varepsilon$ translated into an error of ± 5.4 kPa for the τ_{Sliding} estimate.

5.2. Strain development—*isothermal hold*

Strain in the longitudinal direction is constant during the hold portion of the cure cycle, with the exception of

the temperature dips (Fig. 16). In the transverse direction a decrease in strain is noted, which is assumed to correspond to resin cure shrinkage. Examining the strain gauge behaviour during the temperature dips suggests a sticking condition at the interface. The strain induced by the temperature fluctuation is the same for all gauge locations, whereas if a sliding condition were in effect the gauge response should be proportional to their distance from the interface end.

The degree to which the tool is constrained and/or stretched during the temperature dips reflects the changing modulus of the curing part. This elastic interaction can be quantified by comparing the apparent CTE demonstrated by the tool, to the free CTE of the tool. For the purposes of this discussion, the term *Elastic Constraint* will be defined as follows:

$$\text{Elastic Constraint} = \text{CTE}_{\text{Measured}} - \text{CTE}_{\text{Free}} \quad (26)$$

The theoretical minimum value for the elastic constraint is zero, which would indicate that the tool was not influenced to any degree by the part. The absolute maximum elastic constraint possible is the difference between the CTE of the tool and part, which would occur in the case that the tool was completely dominated by the part. The elastic constraint is measured by the slope of a strain versus temperature plot during a given temperature dip. The development of elastic constraint with respect to part degree of cure is shown in Fig. 17. Each elastic constraint value displayed is the average of the two gauges at the same distance from the part symmetry line. Also shown are lines indicating estimates based on classical lamination theory (CLT), (e.g. Promal [12]), for the longitudinal and transverse directions. Calculations were performed using the fully cured composite properties given in Table 1.

Early in the cure cycle, at a low degree of cure, the elastic constraint is negligible in the transverse direction yet at the same time there is approximately $10 \mu/^\circ\text{C}$ of constraint in the longitudinal direction. With increasing degree of cure the elastic constraint increases in both directions, approaching the estimate for a fully cured composite part.

5.3. Strain development—*heat-up*

The mechanical strain evolution during the heat-up portion of the cure cycle is shown in Fig. 18. Identifying trends in strain development which occur during the heat-up is subtle because the strain magnitudes are relatively small. Prior to 60 min, gauges show no significant response. However, shortly after the first temperature dip, strain measurements at each gauge location start to diverge slightly but relatively consistently. By the time the isothermal hold is reached, the longitudinal gauges show a negative strain approximately proportional to their distance from the tool free end (Fig. 18).

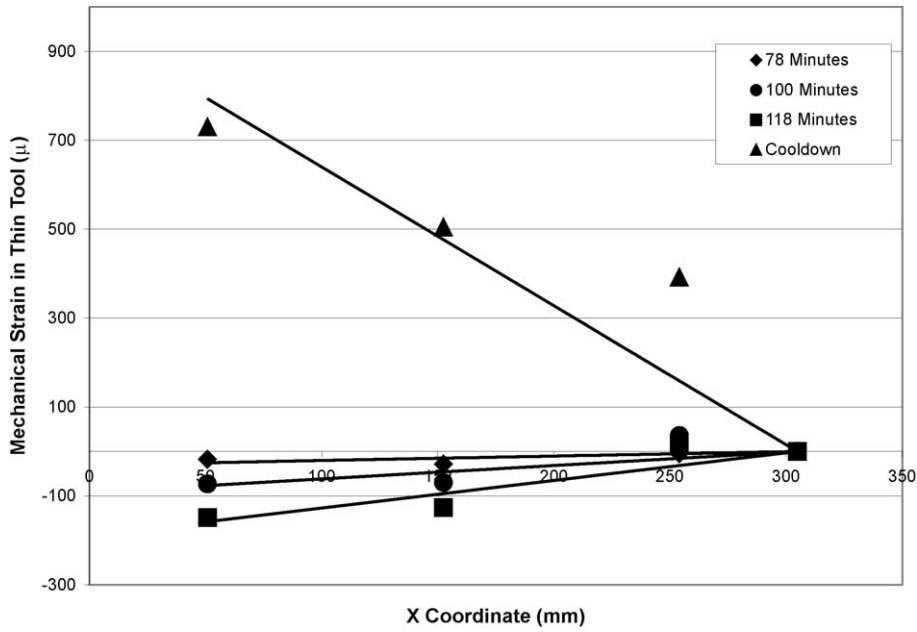


Fig. 15. Strain versus gauge location. The slope of the fitted line is used for calculation of τ_{Sliding} . 586 kPa autoclave pressure/release agent interface.

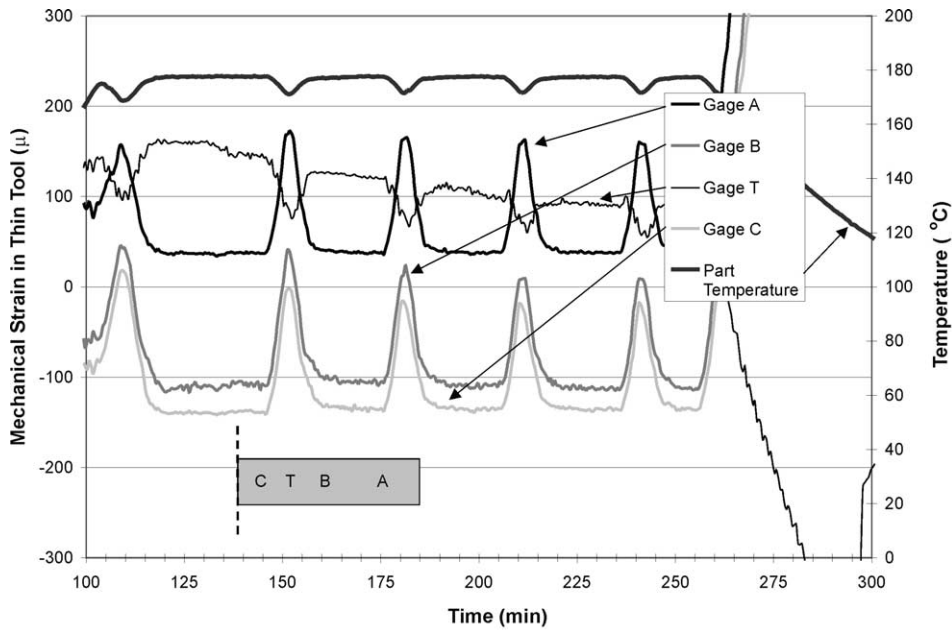


Fig. 16. Mechanical strain evolution during the isothermal hold. 586 kPa autoclave pressure/release agent interface.

As with the post debond strain distribution, this is indicative of a sliding friction condition at the interface. Following the method outlined in Section 5.1, one can estimate an interfacial shear stress corresponding to this strain distribution using the slopes estimated from Fig. 15 and Eq. (25). A plot of τ_{Sliding} against resin degree of cure is shown in Fig. 19 from which it is apparent that τ_{Sliding} is strongly related to the degree of advancement of the resin cure.

5.4. Instrumented results—other experimental conditions

Having examined the results of a single experiment thoroughly, the results from other experimental conditions can be contrasted. The strain versus time plots for the other process and tool surface conditions examined are shown in Fig. 20–22. Again, only gauges on one side of the tool symmetry line are shown for the sake of clarity.

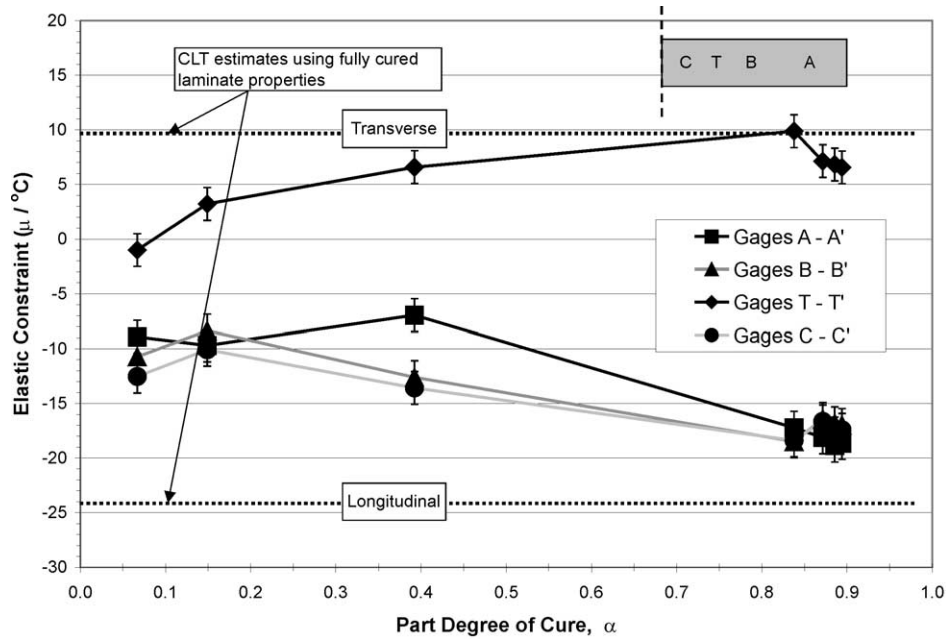


Fig. 17. Elastic constraint plotted with respect to part degree of cure. 586 kPa autoclave pressure/release agent interface.

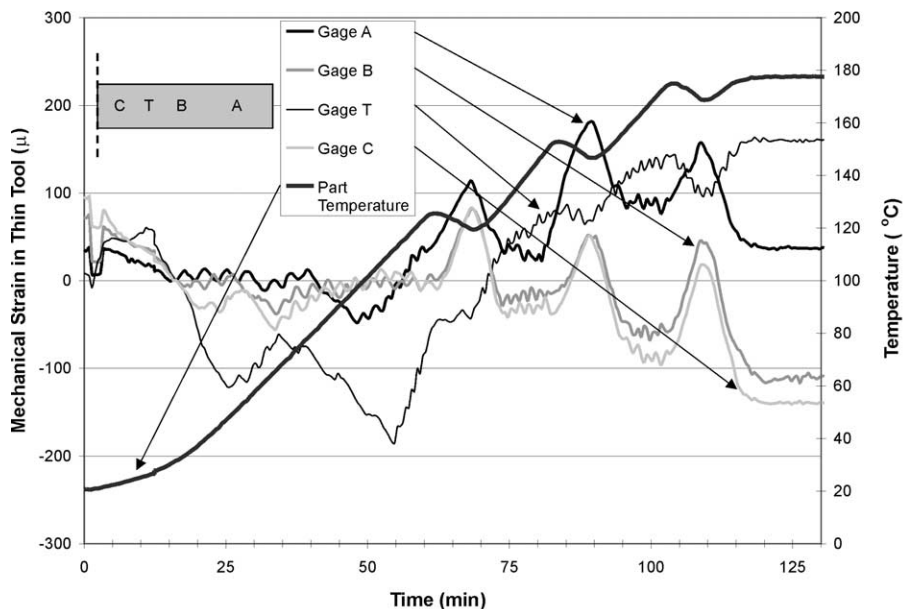


Fig. 18. Mechanical strain evolution during the heat-up portion of the cure cycle. 586 kPa autoclave pressure release agent interface.

5.4.1. Other experimental conditions—heat-up

During the heat-up portion of the cure cycle, the sliding interface condition is dominant for all of the experiments. As before, the evolution of τ_{Sliding} with respect to degree of cure can be examined by first plotting measured strain versus gauge location. A plot of τ_{Sliding} with respect to degree of cure for all experimental conditions is shown in Fig. 23. In all cases τ_{Sliding} increases with increasing resin degree of cure.

By the end of the cure cycle there are substantial differences in τ_{Sliding} between the various experimental conditions, with the value of τ_{Sliding} being much greater

for the higher pressure conditions. Taking into account the error associated with the estimate of τ_{Sliding} as well as the expected variability in this parameter, there is no significant pressure or tool surface effect at the low degrees of cure encountered during the heat-up.

For all experiments, the evolution of elastic constraint during the temperature dips was similar to that depicted in Fig. 17, except for the 103 kPa autoclave pressure/FEP case (Fig. 24). For the other three cases elastic constraint builds with increasing degree of cure, approaching the CLT estimate by the end of the cure cycle. However, for the case of the 103 kPa autoclave

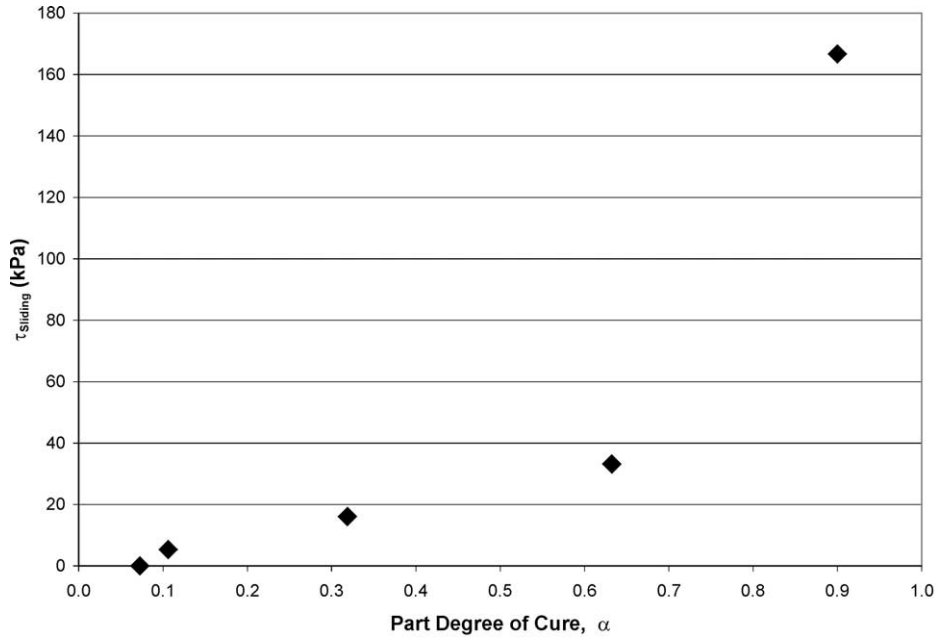


Fig. 19. Change in $\tau_{sliding}$ with respect to part degree of cure. 586 kPa autoclave pressure/release agent interface.

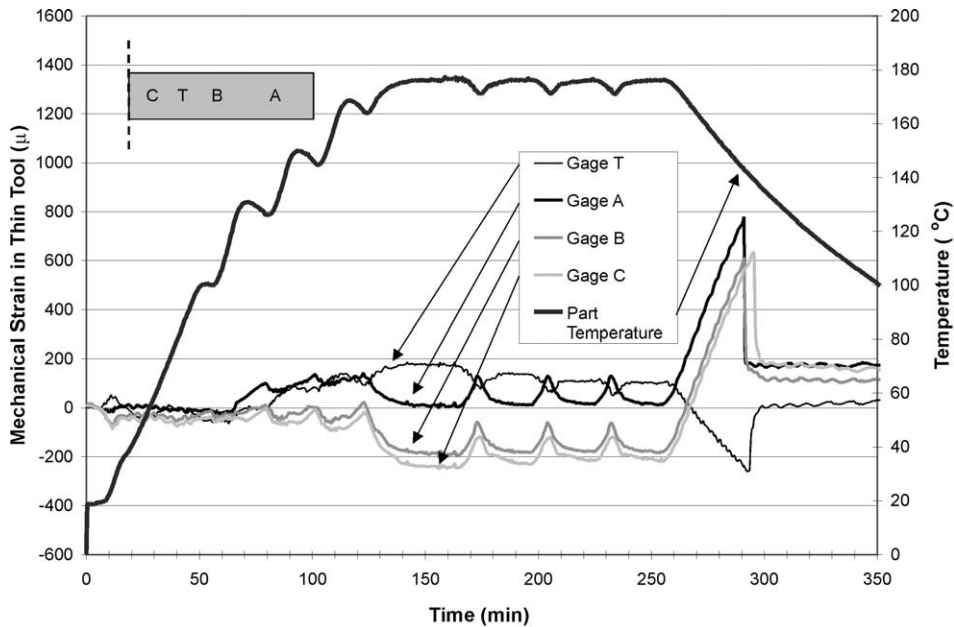


Fig. 20. Instrumented tool mechanical strain development for the entire cure cycle. 103 kPa autoclave pressure/release agent interface.

pressure/FEP condition the term elastic constraint is not strictly correct. As is apparent from Fig. 24, gauge response in the longitudinal direction is proportional to the distance from the end, indicative of a sliding condition. For this experimental case, τ_{Debond} was evidently low enough to be reached during the temperature dips.

5.4.2. Other experimental conditions—*isothermal hold and cool-down*

Gauge response during the isothermal hold was similar for all experimental conditions, except for

during the previously discussed temperature dips. However, during the cool-down marked differences become apparent.

For the case of 103 kPa autoclave pressure/release agent (Fig. 20), as with the previously examined 586 kPa autoclave pressure/release agent condition the tool and part are perfectly bonded at the start of the cool-down. In the low pressure case though, the debond front does not travel at a constant rate along the length of the tool. For gauges A and B, debonding occurs simultaneously, after which the debond front travels at a rate of

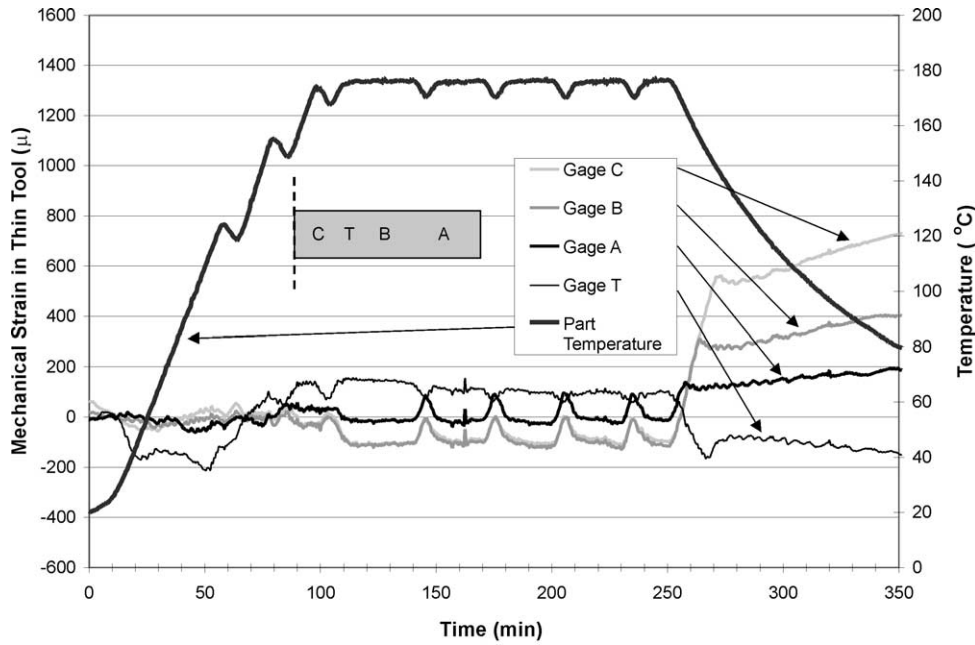


Fig. 21. Instrumented tool mechanical strain development for the entire cure cycle. 586 kPa autoclave pressure/FEP interface.

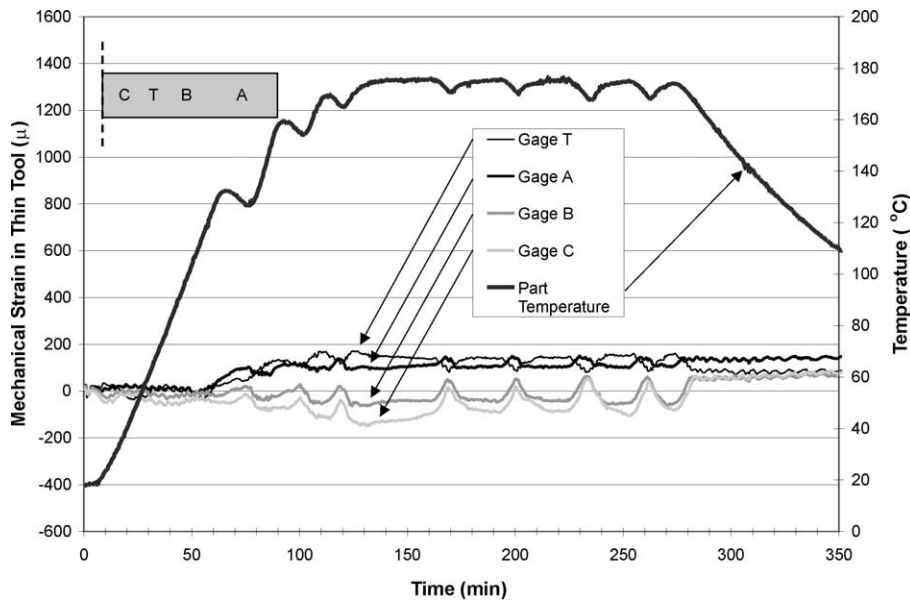


Fig. 22. Instrumented tool mechanical strain development for the entire cure cycle. 103 kPa autoclave pressure/FEP interface.

approximately $26.2 \text{ mm}/^{\circ}\text{C}$. It is apparent that under the low pressure condition, the debonding event does not progress in as stable a manner as under the high pressure condition.

Using the same methods outlined in Section 5.1, L_S and τ_{Debond} can be estimated from the evolution of strain during the debond events. For the 103 kPa autoclave pressure/Release Agent case, L_S and τ_{Debond} were calculated to be 16 mm and 3.0 MPa respectively. These values are not significantly different from those for the 586 kPa autoclave pressure/Release Agent case (14 mm and 3.8 MPa, respectively).

The experiments performed with an FEP interface also show a sticking condition during the initial cool-down (Figs. 21 and 22). In contrast to the release agent cases the transition from a sticking condition to a sliding condition does not have any associated drop in strain for the FEP interface. This result implies that for the FEP interface there is no difference between τ_{Debond} and the previously calculated cool-down values of τ_{Sliding} . Regarding the 586 kPa autoclave pressure/FEP case there is an apparent increase in τ_{Sliding} after the start of the sliding friction condition. This is illustrated in Fig. 21 where after the debond event, the strain in the

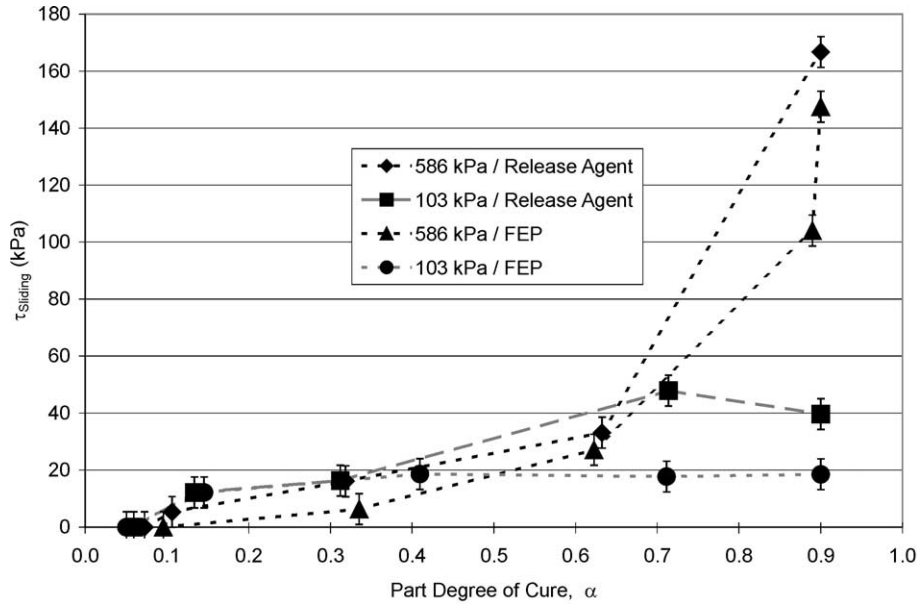


Fig. 23. Change in $\tau_{Sliding}$ with respect to part degree of cure.

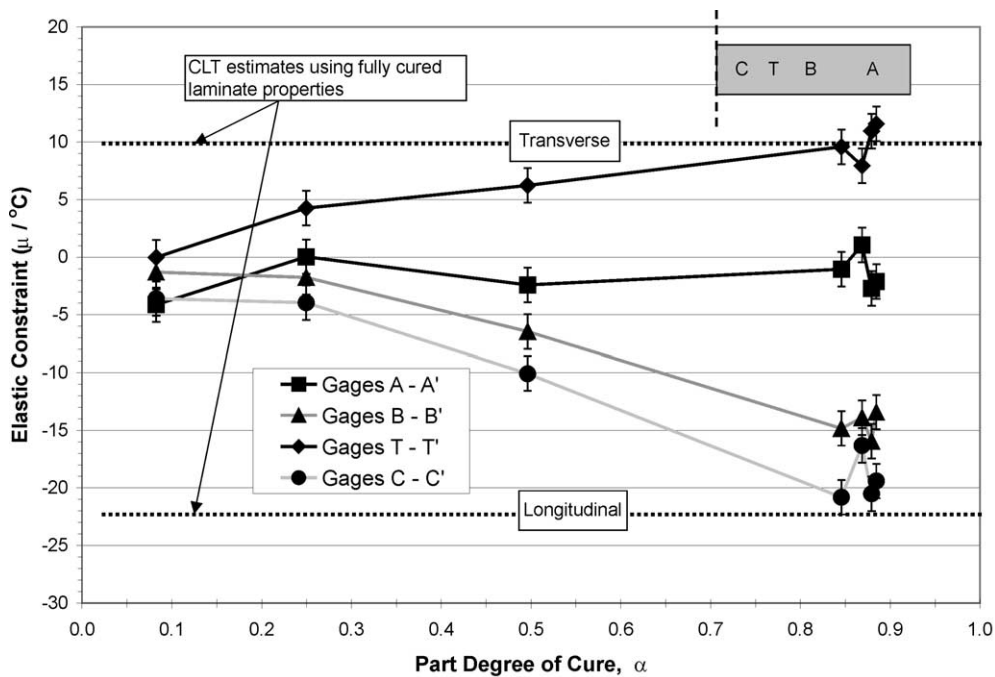


Fig. 24. Elastic constraint with respect to degree of cure. 103 kPa autoclave pressure/FEP interface.

tool increases slightly as the cooldown progresses. The reason for this is not clear but one possibility is that with increasing $\delta_{Interface}$, the FEP layers at the interface may be wrinkling causing an apparent increase in the interface friction coefficient.

6. Discussion

The evolution of the behaviour during the entire cure cycle can now be considered collectively. During the

heat-up portion of the cure cycle all the process conditions exhibit a sliding friction interface condition, with $\tau_{Sliding}$ initially being a negligible value but increasing with resin degree of cure. During the temperature dips the interface behaves elastically, however. An analogy to this behaviour can be drawn by considering a tensile test in which material is taken into the plastic regime. Upon unloading, the material follows a stress-strain path determined by its elastic properties. In the same manner, during the temperature dips the interface behaves elastically until the interfacial shear stress

exceeds τ_{Debond} , after which the interface slides again. Early in the cure cycle it is apparent that $\tau_{\text{Debond}} \approx \tau_{\text{Sliding}}$ because there is no abrupt jump in strain associated with the transition between the two regimes.

During the isothermal hold there is no relative motion between the tool and part and during this period marked differences arise between the FEP and release agent conditions. For the release agent interface, τ_{Debond} increases substantially due to the adhesive characteristic of the curing resin. By the end of the cure cycle, τ_{Debond} has increased to a value several orders of magnitude above τ_{Sliding} . For the FEP interface the impermeable release ply prevents any adhesive bonding between tool and part. During the initial portion of the cool-down the sticking condition operates until the interfacial shear stress builds to τ_{Debond} and debonding occurs, starting at the tool end and travelling towards the centre. After debonding the sliding friction condition dominates again. The evolution of interfacial shear stress versus $\delta_{\text{Interface}}$ is illustrated schematically for release agent and FEP interfaces in Figs. 25 and 26, respectively.

The evolution of τ_{Sliding} and τ_{Debond} with degree of cure has implications with respect to the effect of cure cycle on part shape. The massive tools used in industry often force the temperature ramp rates of the cure cycle to be very low. Because of this, the resin may have already achieved a substantial degree of cure prior to the hold, and hence a higher value of τ_{Sliding} would be operative while still on the heat-up. Alternatively, some cure cycles employ a hold at an intermediate temperature before the ramp to the final cure temperature. It is also possible that during an intermediate isothermal dwell, τ_{Debond} would increase sufficiently to change the interface from a sliding dominated condition to a stick condition. Parts which are subject to these intermediate dwells or slow heat-up rates would be subject to higher interfacial stresses than parts with a single rapid ascent to cure temperature.

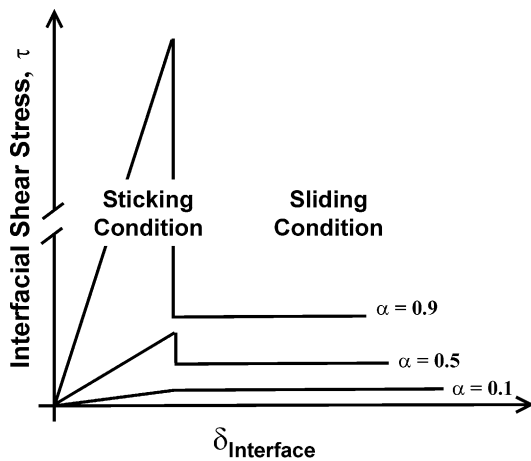


Fig. 25. Schematic illustration of the development of τ_{Debond} and τ_{Sliding} for a release agent interface.

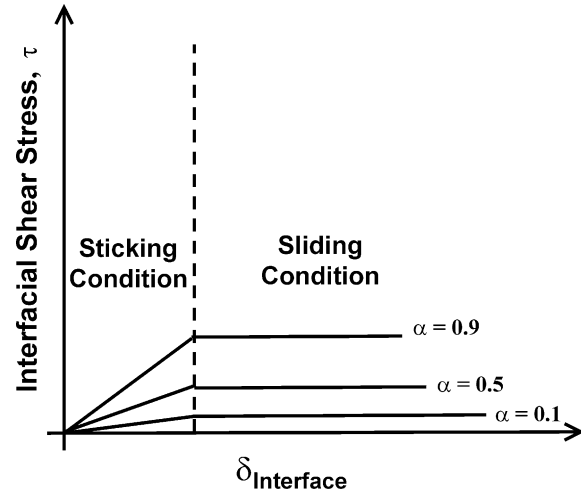


Fig. 26. Schematic illustration of the development of τ_{Debond} and τ_{Sliding} for an FEP interface.

As noted in Section 5.2, even early in the cure cycle while the resin is essentially liquid there is appreciable tool–part interaction in the fibre direction, but little or none in the transverse direction. This is significant in that it indicates a degree of fibre bed interaction with the tool. The majority of researchers assume that prior to gelation, a laminate is unable to develop and store residual stresses, however, fibre bed interaction is a mechanism by which this might occur.

7. Conclusions

1. During the heat-up portion of the cure cycle when part residual stress development due to tool–part interaction is most significant, a sliding friction condition is prevalent at the tool–part interface.
2. The degree of elastic constraint observed at low degrees of cure indicates an interaction between the fibre bed and the tool. This indicates that even prior to resin gelation, the part can develop fibre stresses.
3. The value of τ_{Sliding} increases significantly with degree of cure. During the heat-up, τ_{Sliding} is on the order of 30 kPa, while at the end of the cure cycle values can reach as high as 165 kPa. This suggests that temperature ramp rate or intermediate isothermal dwells can influence interfacial shear stress history and hence change final part shapes.
4. At high degrees of cure τ_{Sliding} is much greater for higher autoclave pressures.
5. A sticking interface condition can occur, particularly during temperature modulations and after isothermal dwells.

6. Adhesive bonding between the tool and part occurs despite the use of release agent on the tool. The τ_{Debond} corresponding to adhesive bonding is on the order of 3–4 MPa.
7. The use of FEP prevents any degree of tool–part adhesive bonding.

Acknowledgements

The authors wish to thank the Natural Sciences and Engineering Research Council of Canada (NSERC) and the Boeing Commercial Airplane Group (Seattle) for their financial support for this research. Past and current members of the Composites Group at The University of British Columbia are recognized for their contribution to our current knowledge of composites processing, process modelling, and the development of software tools for process analysis.

References

- [1] Pagliuso S. Warpage, A. Nightmare for composite parts producers. In: Hayashi T, Kawata K, Umekawa S, editors. Progress in science and engineering of composites, ICCM 4. 1982. p. 1617–23.
- [2] Nelson RH, Cairns DS. Prediction of dimensional changes in composite laminates during cure. In: 34th International SAMPE Symposium. 1989. p. 2397–2410.
- [3] Ridgard C. Accuracy and distortion of composite parts and tools: causes and solutions. SME tech paper, Tooling for Composites '93. 1993.
- [4] Johnston A, Hubert P, Nelson K, Poursartip A, Fernlund G. A sensitivity analysis of modelling predictions of the warpage of a composite structure. In: 43rd International SAMPE Symposium and Exhibition, Anaheim, California. 1998. p. 629–40.
- [5] Melo JD, Radford DW. Modeling manufacturing distortions in flat symmetric, composite laminates. In: 31st International SAMPE Technical Conference. 1999. p. 592–603.
- [6] Hubert P, Poursartip A, Bradley WL. Direct observations of transverse flow in fibre reinforced composite materials during processing. Proceedings of the 11th Technical Conference on Composite Materials of the American Society for Composites 1996:738–47.
- [7] Flanagan R. The dimensional stability of composite laminates and structures. PhD thesis, Queen's University of Belfast; 1997.
- [8] Fernlund G, Rahman N, Courdji R, Bresslauer M, Poursartip A, Willden K, Nelson K. Experimental and numerical study of the effect of cure cycle, tool surface, aspect ratio, and the lay-up on the dimensional stability of autoclave-processed composite parts. *Compos Part A* 2002;33:341–51.
- [9] Crasto A, Kim RY, Russell JD. In situ monitoring of residual strain development during composite cure. 44th International SAMPE Symposium 1999:1706–17.
- [10] Johnston A, Vaziri R, Poursartip A. A plane strain model for process-induced deformation of laminated composite structures. *J Compos Mat* 2001;35(16):1435–69.
- [11] Reddy JN, Roy S. Finite element analysis of adhesive joints. In: Lee LH, editor. Adhesive bonding. New York: Plenum Press; 1991.
- [12] Kaw AK. Promal (1.0) Boca Raton. CRC Press; 1997.